A Breakage and Adhesion Regime Map for the Normal Impact of Loose Agglomerates with a Spherical Target

Duy Nguyen and Anders Rasmuson
Chemical and Biological Engineering, Chalmers University of Technology, SE-412 96 Gothenburg, Sweden

Kyrre Thalberg and Ingela Niklasson Björn
AstraZeneca R&D Centre, SE-431 83, Mölndal, Sweden

DOI 10.1002/aic.14922
Published online July 16, 2015 in Wiley Online Library (wileyonlinelibrary.com)

Discrete element method-based analysis is conducted to investigate the effects of interface energy between particles on the breakage and adhesion of loose agglomerates upon impact with a spherical target. A mechanistic approach is tested to find a relationship between particle properties, kinetic energy, and the agglomerate structure after the impact, which resulted in a new dimensionless number, the ratio of the two interface energies. In combination with Δ*, a dimensionless number relating incident kinetic energy to agglomerate strength (Moreno-Atanasio and Ghadiri M,* Chem Eng Sci. *2006;61(8):2476–2481), a good description of the agglomerate impact is obtained. The agglomerate structure after impact is mapped using the two dimensionless numbers and is in good agreement with experimental observations. The constructed regime map can serve as a guide for selecting preliminary process parameters in adhesive particle mixing.*
 AIChE J, 61: 4059–4068, 2015
Keywords: breakage, adhesion, regime map, loose agglomerates, DEM

Introduction

Agglomerates of fine particles are commonly used as intermediate and final products in a wide array of industries to improve the flowability, the homogeneity, and the handling properties of desired components.[1] During processing, the agglomerates of fines may get exposed to different mechanisms involved in the formulation process, for example, disintegration, dispersion, and granulation. The strength of agglomerates, thus plays an important role in delivering product performance. For instance, in dry powders for inhalation, the agglomerates are disintegrated and adhered onto carrier particles to obtain a certain structure that should be strong enough to survive during handling and loose enough to be entirely dispersed during inhalation.[2,3] Therefore, controlling the agglomerate strength for the ease of processing as well as for the stability of final products is highly desirable in powder manufacturing.

Due to the difficulties that arise at small length and time scales, as well as the high degree of freedom in agglomeration and deagglomeration, discrete element method (DEM) simulation has become the primary choice for investigating agglomerate impact[4] and particulate flow in granular mixers.[5] Several DEM-based studies of the breakage of agglomerates can be found in the literature.[6–8] These studies show that interparticle properties are critical factors governing agglomerate strength, in addition to primary particle properties. Mechanistic models have also been used to relate the interface energy between particles to breakage behavior.[9,10] Although the nature of breakage fragments after impact has significant importance in a variety of processes, for example, dry particle coating, very few in-depth studies on post-impact have been documented. A recent study[11] shows that the adhesion and the structure of breakage fragments can be controlled by adjusting impact velocity. In that work, the interface energies between fine particles and between fine and carrier particles were kept constant.

In this work we will, in detail, explore the effects of interface energies, not only on agglomerate breakage but also on the adhesion of breakage fragments onto a target. Using DEM simulations, the effects of the interface energy between fines and the target, which has often been neglected in previous studies, is specifically taken into account and varied. A mechanistic approach is introduced to establish a relationship between the physical properties of primary particles and the agglomerate structure in the final state of the impact, for example, fragment size, the fraction of fines captured by the target, and the thickness of fines covering the surface. In order to generalize and utilize the results, regime maps for the corresponding characteristics have been constructed using two dimensionless numbers, the ratio of the two interface energies and the previously proposed Δ number,[9] to serve as a guideline for selecting preliminary operating conditions and to provide a prediction of impact behavior.

Methodology

Single collisions between fine-particle agglomerates and a spherical target (the carrier particle) were simulated using

Correspondence concerning this article should be addressed to A. Rasmuson at rasmuson@chalmers.se.

Table 1. Physical Properties of the Primary Fine Particle and the Carrier

Parameters	Fine Particle	Carrier Particle
Particle size	5 μm	200 μm
Particle density	1520 g/m^3	1490 g/m^3
Young modulus	4 GPa	0.1 GPa
Poisson ratio	0.12	0.29
Friction coefficient	0.26	0.3
Rolling friction coefficient	0.002	0.002
Restitution coefficient	0.5	0.89

Table 2. Agglomerate Properties

Agglomerates with $\Gamma_{1\text{-}1}$ (J/m^2) of	0.005	0.01	0.015	0.02	0.03
Radius (mm)	0.0307	0.0305	0.0302	0.0301	0.0300
Packing fraction	0.540	0.550	0.567	0.572	0.578
Number of contacts	4660	4706	4774	4888	4920

DEM where the movement of individual particles is tracked using Newton's equation of motion

$$m_i \frac{d^2 x_i}{dt^2} = F^{ij}_{\text{contact}} + F^{i}_{\text{gravity}} + F^{i}_{\text{fluid}} \tag{1}$$

$$I_i \frac{d\omega_i}{dt} = T^{i}_{\text{contact}} \tag{2}$$

where F^{ij}_{contact}, F^{i}_{gravity}, F^{i}_{fluid} are the contact force between particles *i*-*j*, the gravity force, and the fluid force that act on particle *i*. I_i, ω_i, and T_i are the inertia moment, the angular velocity and the torque that act on particle *i*.

Particle gravity has been neglected as it is several orders of magnitude less than the contact force acting on the fine particles. In the context of this study, no fluid flow is taken into account. The elastic-cohesive contact force between two particles *i*,*j* is modelled using the JKR theory[12] which describes the contact radius *a* as

$$a^3 = \frac{3R_{i-j}}{4E_{i-j}}\left(F_{ne} + 3\pi\Gamma_{i-j}R_{i-j} + \sqrt{6\pi\Gamma_{i-j}R_{i-j}F_{ne} + \left(3\pi\Gamma_{i-j}R_{i-j}\right)^2}\right) \tag{3}$$

where $\Gamma_{i\text{-}j}$ is the adhesion work, that is, the work per unit area needed to separate two surfaces in vacuum, F_{ne} is the normal elastic-cohesive contact force. The effective radius $R_{i\text{-}j}$ and the effective Young modulus $E_{i\text{-}j}$ are defined as

$$\frac{1}{E_{i-j}} = \frac{1-\nu_i^2}{E_i} + \frac{1-\nu_j^2}{E_j} \tag{4}$$

$$\frac{1}{R_{i-j}} = \frac{1}{R_i} + \frac{1}{R_j} \tag{5}$$

where E_i, R_i, ν_i are the Young modulus, the radius and the Poisson ratio of particle *i*. The detailed simulation framework can be found in Nguyen et al.[11]

To set up the initial state, loose agglomerates were formed with 1000 spherical fine particles with the physical properties shown in Table 1. For pairwise parameters, for example, restitution and friction coefficients, the values in the columns are shown for fine-fine and fine-carrier pairs, respectively. A centripetal force field was applied to all the primary particles, which were randomly located in a spherical space, to initiate agglomeration. At the start, an agglomerate was created with the lowest interface energy between fines ($\Gamma_{1\text{-}1}$), that is, 0.005 J/m^2, until all the primary particles had reached their stable positions. Other agglomerates were then generated by introducing the desired interface energies in very small time steps to avoid the accumulation of residual stress within the agglomerates. By this approach, agglomerates having the same packing density but differing in interaction between fines was obtained, as shown in Table 2. The contact histogram (Figure 1) also shows that the agglomerates are well-packed and the distribution is similar for different assemblies. The agglomerates were then guided to perform a normal impact with the carrier particle at different impact velocities. The initial set up and the final state after impact is illustrated in Figure 2. The interaction between fines and the carrier ($\Gamma_{1\text{-}2}$) was varied for each collision. The details of the simulations are shown in Table 3.

In the present study, several parameters were used to describe the breakage and the adhesion behavior in the final state of the impact (see Figure 2b). The first and the second largest surviving fragments were used as a complement to the damage ratio[13] in characterizing breakage performance. The adhesion of breakage fragments onto the surface of the carrier particle was characterized by the capture ratio and the thickness of the fines. The capture ratio was defined as the fraction of fine particles captured by the target to the total number of fine particles in the initial agglomerate. The thickness of fines was estimated by the fraction of adhered particles that are in direct contact with the carrier (the first layer), to the total number of fines that is captured by the target.

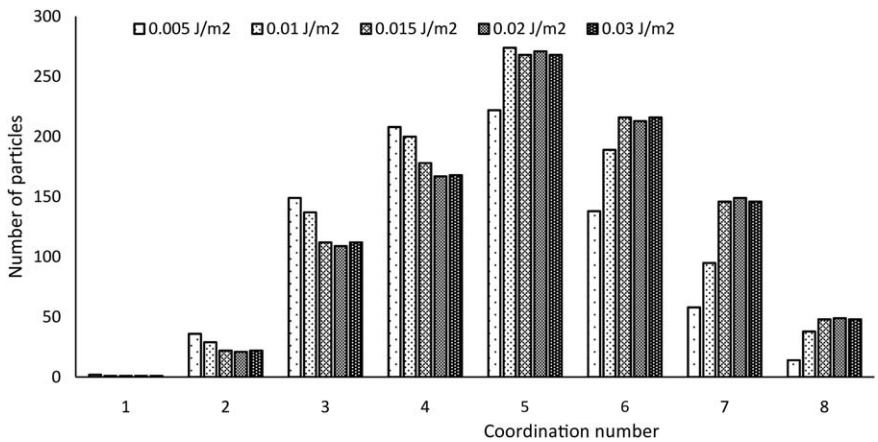

Figure 1. Contact histogram of five agglomerates.

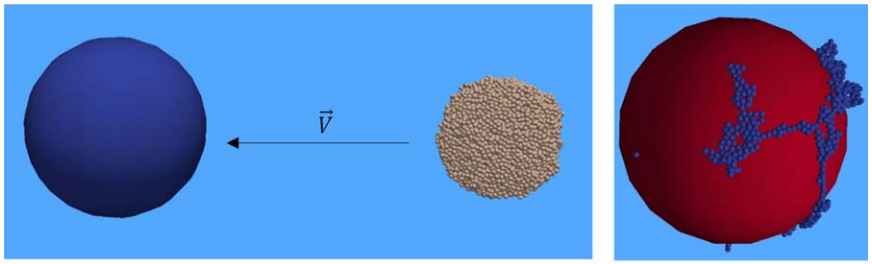

Figure 2. Simulated system (a) before impact, (b) after impact, fines are attached on the carrier surface.

[Color figure can be viewed in the online issue, which is available at wileyonlinelibrary.com.]

Results and Discussion

Effects of interface energies on the breakage of agglomerates

To describe the breakage behavior of agglomerates, a combination of the damage ratio and the first and the second largest fragment size is recommended, since, for the same value of the damage ratio, the breakage may introduce different patterns.[14] The dependence of the first and the second largest fragment on the impact velocity is shown in Figures 3 and 4 corresponding to different interface energies between fines-fines ($\Gamma_{1\text{-}1}$) and between fines-carrier ($\Gamma_{1\text{-}2}$), respectively. The fragments were distinguished using a clustering algorithm[15] and their size has been normalized with the original size of the agglomerates. It should be noted that for a real agglomerate, $\Gamma_{1\text{-}1}$ would affect the packing density within the agglomeration process, and obviously, breakage behavior would also be influenced. In this study, however, the packing density is almost identical for different agglomerates and all the agglomerates have approximately the same number of initial interparticle bonds (see Table 2). Consequently, the nature of the breakage can be determined by the amount of kinetic energy spent for breaking a single contact including adhesion, and normal and tangential damping. In Figure 3, the increase in $\Gamma_{1\text{-}1}$ results in larger surviving fragments, as the interparticle bonds have been enhanced to survive under the external forces exerted on them during impact. It can also be seen that the impact velocity facilitates the breakage performance due to the increase in available kinetic energy. The difference of the largest surviving fragments between investigated cases follows the same trend within the covered range of the impact velocity due to the fact that the breakages of all the agglomerates fell within the same regime range, that is, microscopic to macroscopic.[8] The regimes beyond these, for example, disintegration, are not of interest here, since no fines will be captured at extremely high impact velocity. The breakage shows strong dependence on the impact velocity at low velocities, and approaches an asymptotic behavior at higher velocities. This characteristics can be explained in terms of the dissipation of energy during impact,[8] that is, a major amount of incident kinetic energy is consumed by contact damping, which increases at high impact velocity. Therefore, the addition of incident kinetic energy due to the use of high impact velocities is not efficiently used for breaking adhesive inter-particle bonds.

Although the effect of $\Gamma_{1\text{-}1}$ is commonly investigated, the influence of the target particle on agglomerate impact has not been reported. It is obvious that fines-carrier interaction is responsible for the adhesion of fines onto a target, however, Figure 4 also features noticeable effects of $\Gamma_{1\text{-}2}$ on the agglomerate breakage. It can be seen that the breakage is facilitated when the agglomerate impacts with a target that has less adhesion with primary fine particles. Although the contact force exerted on the agglomerate upon impact is altered by the surface properties of the target, for example, target elasticity or roughness, only minor changes in breakage performance can be expected, as only surface energy has been adjusted in the studied cases. The time-dependence of the damage ratio, corresponding to the impacts with different values of $\Gamma_{1\text{-}2}$, is shown in Figure 5 ($\Gamma_{1\text{-}1} = 0.01$ J/m^2). It can be seen that on impact with the carrier at a certain velocity, the agglomerate experiences the same greatest deformation regardless of the difference in $\Gamma_{1\text{-}2}$. The variation in the damage ratio, that is, the breakage behavior, in the final state, is thus governed by the restructuring of the breakage fragments after the greatest deformation has been achieved.[11] When the fragments are captured by the target, they tend to stay within the vicinity of the contact area and merge with their neighbors to form larger fragments. The final fragment size thus increases and is varied for different $\Gamma_{1\text{-}2}$. In the event of low $\Gamma_{1\text{-}2}$, fine-particle

Table 3. Details of Studied Cases

$\Gamma_{1\text{-}2}$ (J/m^2)	0.001	0.003	0.005	0.01	0.02	0.03
$\Gamma_{1\text{-}1}$ (J/m^2)	0.005	0.01	0.015	0.02	0.03	
V (m/s)	0.4	0.5	0.5	0.5	0.5	
	0.5	1	1	1	1	
	0.7	1.5	1.5	1.5	1.5	
	1	2	2	2	2	
	1.3	2.5	2.5	2.5	2.5	
	1.5	3	3	3	3	
	1.7	3.5	3.5	3.5	3.5	
	2	4	4	4	4	
	2.5		4.5	4.5	4.5	
	3			5	5	
	3.5				5.5	
					6	

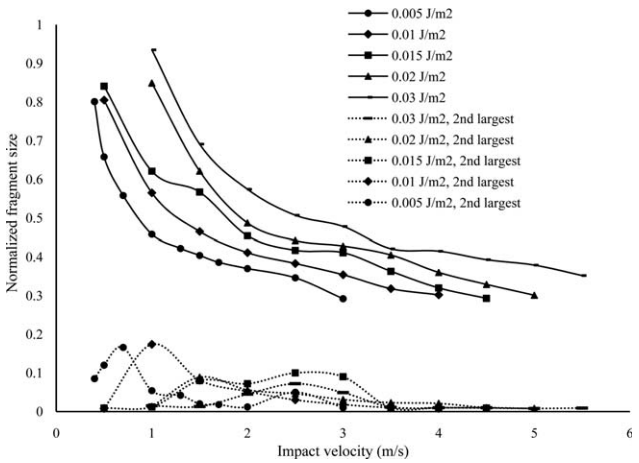

Figure 3. Effects of Γ_{1-1} on the two largest fragment sizes.

fragments are not captured and continue to be distributed, and consequently, breakage performance will be enhanced.

Effects of interface energies on the adhesion of fines onto carrier surface

The dependence of the capture ratio on $\Gamma_{1\text{-}2}$ and $\Gamma_{1\text{-}1}$ is shown in Figures 6–8. High impact velocity generally results in fewer fines adhering onto the carrier surface due to the increase in incident kinetic energy. In Figure 6, a higher $\Gamma_{1\text{-}2}$ indicates that a larger number of fines have been captured by the target. It is due to the fact that the enhanced strength of inter-particle bonds is able to dissipate more kinetic energy of fines. The dependency of adhesion on the impact velocity is similar to that of breakage, that is, strong dependence at low impact velocities and asymptotic behavior at high impact velocities.

$\Gamma_{1\text{-}1}$ shows a more complex effect on adhesion. Two opposite behaviors can be observed that correspond to low and high $\Gamma_{1\text{-}2}$. Figure 7 shows that when there is strong interaction between fines and the carrier particle, an increase in $\Gamma_{1\text{-}1}$ results in a higher capture ratio, that is, more fines are attached onto the carrier surface, and vice versa. Figure 8 depicts the

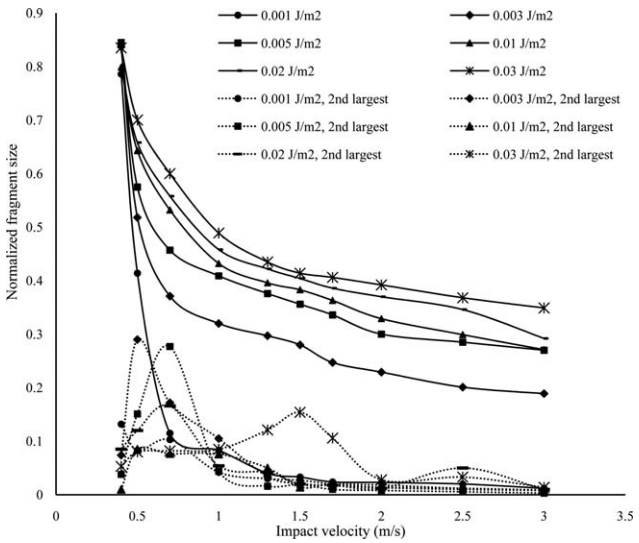

Figure 4. Effects of Γ_{1-2} on the two largest fragments.

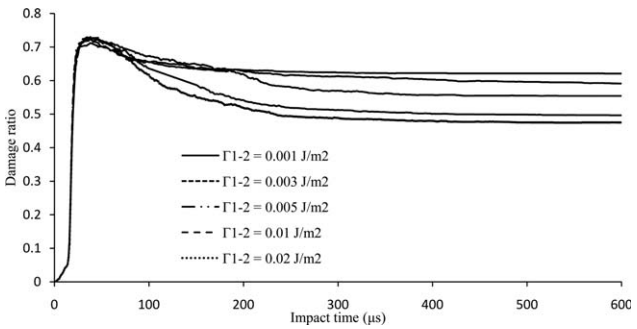

Figure 5. Time dependence of the damage ratio, 2.0m/s, $\Gamma_{1-1} = 0.01 J/m^2$.

The effects of fine-carrier interaction can be observed.

results for weak interaction between fines and the carrier particle, and illustrates the opposite behavior, that is, more fines are captured upon the impact of low $\Gamma_{1\text{-}1}$ agglomerates. These phenomena can be understood by coupling adhesion to breakage behavior. At a certain impact velocity, the agglomerates with high $\Gamma_{1\text{-}1}$ break into larger fragments, as shown in Figure 3. When the adhesion between fines and the carrier particle is strong enough to dissipate the high kinetic energy of these large fragments, cf. Figure 7, a larger number of fines will be captured by the target. In the event of weak interaction between fines and carrier particle, cf. Figure 8, only small fragments with low kinetic energy will be captured, and consequently, more fines will adhere to the target upon the impact of lower $\Gamma_{1\text{-}1}$ agglomerates. The main feature of Figures 6–8 is that the relative magnitude of $\Gamma_{1\text{-}1}$ and $\Gamma_{1\text{-}2}$ plays an important role in characterizing the impact behavior.

Mechanistic analysis

Figures 3–8 showed that the impact velocity and the interface energies affect the breakage and the adhesion of agglomerates in a complex pattern. A relationship between them is therefore needed to better describe and predict the impact as well as the resulting structure of adhered fragments. For this purpose, a mechanistic approach was employed for analyzing the impact event. Figure 9 shows that the total energy loss is linear with the incident kinetic energy regardless the values of interface energies. This fact motivates the use of the dimensionless number Δ[9] which relates the kinetic energy to the agglomerate strength, $\Delta = \frac{\rho D^{5/3} V^2 E^{2/3}}{\Gamma^{5/3}}$, to describe the breakage of the agglomerate. Since it was shown that the relative magnitudes of the two interface energies governs the impact (see Figures 5 and 6), we propose to use the ratio $\frac{\Gamma_{1-1}}{\Gamma_{1-2}}$, that is, the cohesion strength to the adhesion strength, in combination with the Δ number to couple the breakage and the adhesion of

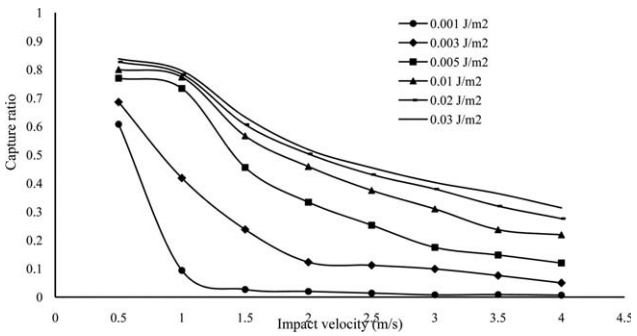

Figure 6. Effects of Γ_{1-2} on capture ratio, $\Gamma_{1\text{-}1} = 0.01$ J/m^2.

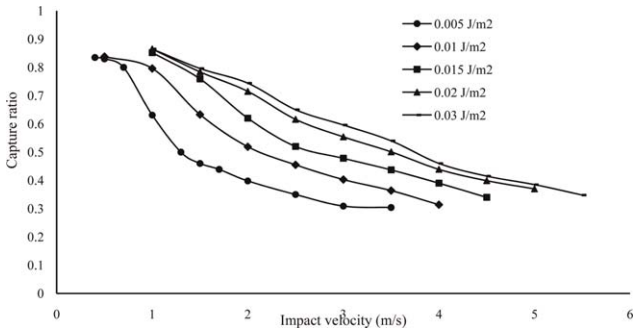

Figure 7. Effects of $\Gamma_{1\text{-}1}$ on capture ratio, $\Gamma_{1\text{-}2} = 0.03$ J/m^2

the agglomerate. In order to test their capability in the description of the impact event, Figures 10–12 show the largest fragment size (i.e., the breakage), the capture ratio (i.e., the adhesion), and the thickness of fines on the carrier surface (i.e., the structure) as a function of the Δ number, corresponding to different combinations of $\Gamma_{1\text{-}1}$ and $\Gamma_{1\text{-}2}$ giving the same ratio $\frac{\Gamma_{1-1}}{\Gamma_{1-2}}$.

As shown, there is good unification of the resulting largest fragment sizes from impacts with the same interface energy ratio (see Figure 10, the ratio of interface energies of 0.5). The same observation also goes for the capture ratio and the thickness of fines in Figures 11 and 12, respectively. The data unification exists not only at low values of Δ, that is, low impact velocities, but also at high values of the Δ, that is, high impact velocities, in a wide range of the interface energies (from 0.005 J/m^2 to 0.03 J/m^2). This analysis shows that it is feasible to relate the characteristics of the agglomerate impact (e.g., fragment size, capture ratio) to primary particle properties (e.g., surface energy, elasticity) and impact parameters (e.g., velocity) in terms of a mechanistic description. Although the dimensionless number Δ is known for its possibility in the description of the damage ratio,[9] it can be further considered to also describe the fragmentation and the post-impact structure of the agglomerate, which is more important in practice. For this purpose, the incorporation of this number and the interface energy ratio is an important key to include the effect of the target on the agglomerate deformation and the adhesion of breakage fragments. However, it should be noted that the linear behavior of the energy loss (see Figure 9), which is essential in the derivation of the Δ number, holds only for the investigated cases, that is, within the microscopic and the macroscopic regimes. At extreme regimes such as disintegration, the energy dissipation during impact introduces different

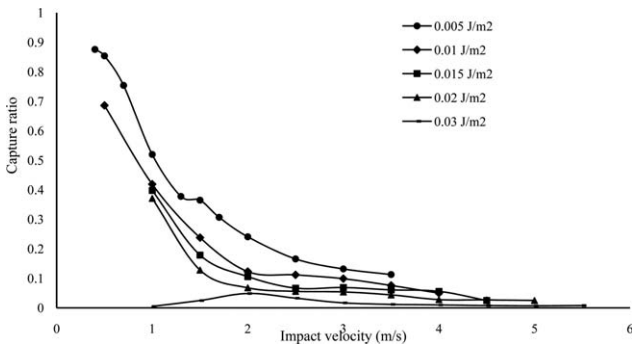

Figure 8. Effects of $\Gamma_{1\text{-}1}$ on capture ratio, $\Gamma_{1\text{-}2} = 0.003$ J/m^2

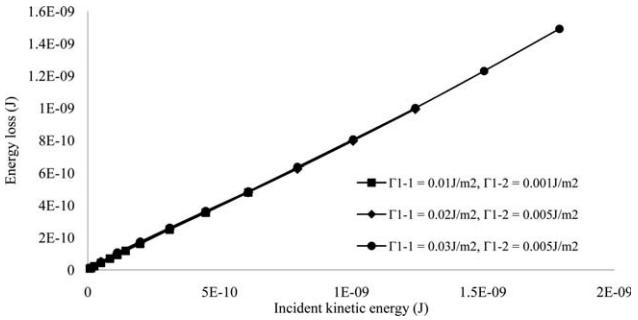

Figure 9. Energy loss as a function of incident kinetic energy for different combinations of the surface energies.

Linear relationship can be observed.

mechanisms, as pointed out by Moreno-Atanasio,[8] consequently, the Δ and the interface energy ratio may not be able to relate particle properties and impact parameters to the breakage of agglomerates. Also, for instances in which there is no noticeable adhesion of fragments onto a target, for example, at high impact velocity or very low $\Gamma_{1\text{-}2}$, the effect of fines-carrier interaction on the breakage performance can be neglected and the interface energy ratio is consequently not applicable. It should be noted that the unification behavior in Figures 10–12 is also observed for other cases which corresponds to different values of the ratio of the interface energies from 0.16 to 30.0.

Breakage—adhesion regime map

Based on the analysis of the simulation results, regime maps for the breakage—adhesion event can be constructed using the proposed dimensionless numbers, that is, the Δ number and the ratio of interface energies $\frac{\Gamma_{1-1}}{\Gamma_{1-2}}$. From a mechanistic point of view, the Δ number describes the effects of $\Gamma_{1\text{-}1}$ on agglomerate strength. In combination with the interface energy ratio, the dimensionless numbers describe the fraction of incident kinetic energy spent for breaking inter-particle bonds between fines and the fraction of energy loss due to fine-carrier interaction. The corresponding regimes for the largest fragment size, the capture ratio, and the thickness of fines are illustrated in Figures 13–15, respectively. In these figures, the curves illustrate the corresponding characteristics as a function of the Δ number at constant interface energy ratios.

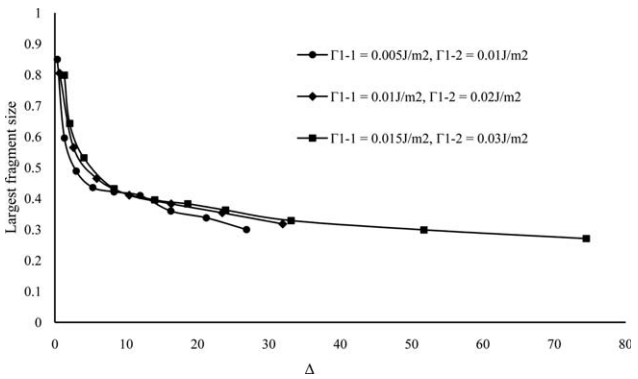

Figure 10. Relationship between the largest fragment size and the dimensionless group Δ, at the interface energy ratio = 0.5.

Data unification can be observed.

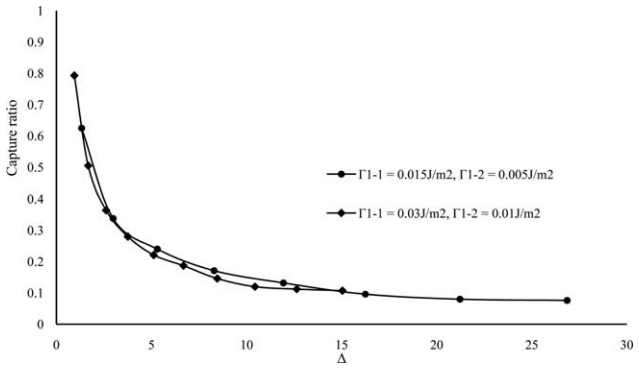

Figure 11. Relationship between the capture ratio and the dimensionless group Δ, at the interface energy ratio = 3.

Data unification can be observed.

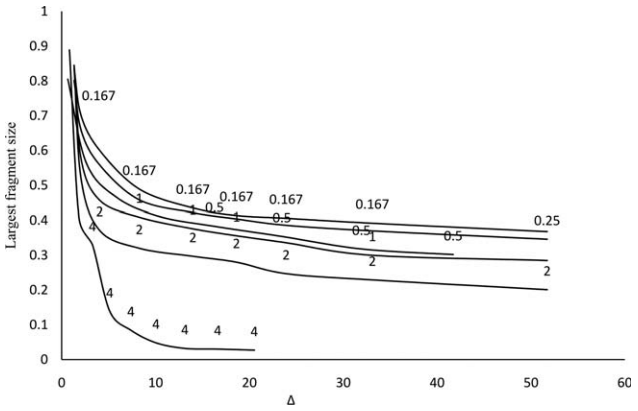

Figure 13. The largest fragment as a function of Δ, at constant interface energy ratios indicated by numbers.

In Figure 13, the largest fragment size is sensitive to the Δ number at low values before it approaches asymptotic behavior at high values of Δ. The fragment size decreases with an increase in Δ, which implies either an increase in the impact velocity or a decrease in $\Gamma_{1\text{-}1}$, that is, an increase in the available energy spent on breaking inter-particle bonds. The sensitivity of fragment size to the Δ number can be related to the energy dissipated during impact, i.e, the energy consumed for breaking adhesion bonds is not utilized at high impact velocity. It is shown in Figure 13 that a better breakage performance can be obtained at a higher interface energy ratio. This behavior can be understood by considering two cases, one at constant $\Gamma_{1\text{-}1}$ and one at constant $\Gamma_{1\text{-}2}$. In the first case, the dependence of the largest fragment size on the interface energy ratio can be explained in analogy to the effects of $\Gamma_{1\text{-}2}$, that is, weak interaction between fines and carrier particle facilitates breakage performance. The second case, in which an increase in $\Gamma_{1\text{-}1}$ results in a reduction of fragment size, should be considered in combination with the impact velocity that appears in the Δ number. When $\Gamma_{1\text{-}1}$ increases, the impact velocity should follow the same trend to maintain the same value of Δ, consequently, more kinetic energy will be available in the system. In other words, adhesion is inadequate which will result in better breakage performance, as earlier discussed.

Figure 14 shows two regimes for the adhesion of fines onto the surface of a carrier particle. At low values for the interface energy ratio, the capture ratio is reduced with increasing Δ number due to the increase in available kinetic energy. A distinct behavior can be observed at extremely high values of the interface energy ratio, which corresponds to the case with strong interaction between fines and weak interaction between fines and the carrier. At low values of the Δ number, the capture ratio increases with the increase in Δ, which implies either higher impact velocity or less $\Gamma_{1\text{-}1}$. This means that the use of low impact velocity is not able to fragmentize strong agglomerates, consequently, large fragments containing high kinetic energy cannot be captured by weak interaction with the carrier particle. Therefore, an increase in the Δ number will produce finer fragments that can be attached by the carrier. If the simulations are extended to extremely low values of the Δ number, similar behavior can be expected for low values of interface energy ratio since no breakage will occur. Such behavior that higher capture ratio is obtained at lower interface energy ratio can be understood within the discussion given for Figure 13.

The fraction of fines in direct contact with the carrier in the final state can be used as an index of the thickness of fines that cover the target, that is, a higher fraction indicates a thinner layer of fines. Figure 15 shows that the thickness of fines is reduced with increasing Δ number. This is the result of greater

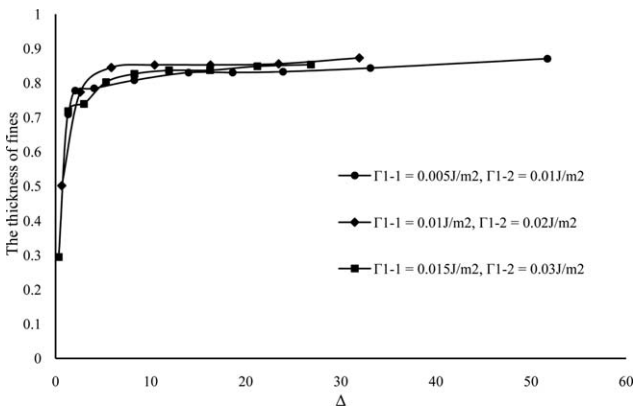

Figure 12. Relationship between the thickness of fines and the dimensionless group Δ, at the interface energy ratio = 0.5.

Data unification can be observed.

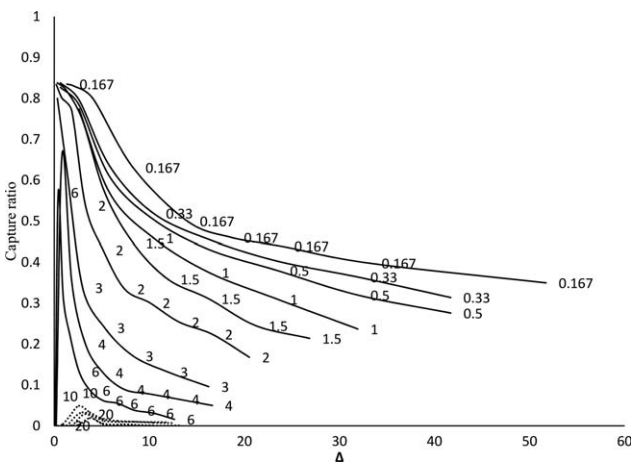

Figure 14. The capture ratio as a function of Δ, at constant interface energy ratios indicated by the numbers.

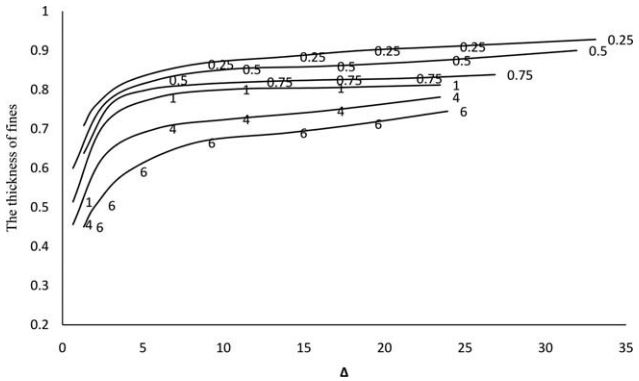

Figure 15. The thickness of fines as a function of Δ, at constant interface energy ratios indicated by the numbers.

breakage performance which generates finer fragments. The use of high interface energy ratios, which generates smaller fragments, provides a thicker layer of fines. The effects of the interface energy ratio on the thickness of fines are therefore in contrast to such effects on the fragment size. This may be due to the fact that the interface energy ratio introduces an influence on the size ratio of fragments. The sensitivity of the thickness of fines to the Δ number has also been found to increase at high interface energy ratios. Consequently, a more detailed analysis is needed to study these mechanisms.

The structure of breakage fragments that adhere to the target has been mapped and is shown in Figure 16 as functions of the dimensionless number Δ and the interface energy ratio $\frac{\Gamma_{1-1}}{\Gamma_{1-2}}$. In Figure 16, nine regimes are distinguished based on values of the fragment size and the capture ratio (indicated by the solid lines) and values of the fraction of fines in the first layer (indicated by the dashed lines). In this work, fragments with normalized size greater than 0.5 are considered as large ones whilst others with normalized size less than 0.2 are considered as small ones. Thin and thick layer of fines on the target are limited by the fraction of fines in the first layer higher than 0.8 and less than 0.6, respectively.

Experimental data were generated to support the general observations in the constructed regime map. To evaluate the resulting structures corresponding to the change of the interface energy ratio, two mixtures with different fine—carrier interaction were prepared. Figure 17 shows the SEM images taken from the mixing of micronized active pharmaceutical ingredient (API) with (a) lactose carrier and (b) lactose carrier coated with a thin layer of Magnesium stearate (MgSt) at two different mixing times. The addition of MgSt is known to weaken the API-carrier interaction.[16] The two blends were prepared at the same mixing intensity in a turbula mixer, with the same API load of 5% w/w. While the interaction between API particles is similar, the main difference between samples is the change in the interface energy ratio $\frac{\Gamma_{1-1}}{\Gamma_{1-2}}$, which will be high for coated carrier and low for uncoated carrier. The capture ratio, that is, the amount of API on the carrier surface, and the relative thickness of API are the main parameters of interest. It is clear from Figure 17 that a great number of small API fragments can be found on the uncoated carrier particles and they tend to be mashed over the surface (a). In contrast, the coated carrier hosts larger and thicker fragments whilst leaving more free space on the surface (b). This is in good agreement with the regime map (Figure 16), where a thicker layer and a lower capture ratio is predicted at a higher interface energy ratio $\frac{\Gamma_{1-1}}{\Gamma_{1-2}}$. A comparison at short mixing time for uncoated (c) and coated (d) carriers further indicates that the interface energy ratio plays an important role as regards the capture of fines. Quite few API fragments can be found in the case of weak interaction (d) and at the same time a large agglomerate that has only been partially fragmented is observed (Figure 17d, bottom right).

Experimental data adopted from the literature are employed to study the resulting structures corresponding to different values of the Δ number. Sato et al.[17] carried out the mixing of sugar particles and MgSt as host and guest particles at different mixing rates to study the effects of mixing intensity (the Δ number) on the structure of covering fines. After 60 s of mixing, it was reported that MgSt formed discrete fragments on host particles at lower mixing rate (500 rpm), while a smooth

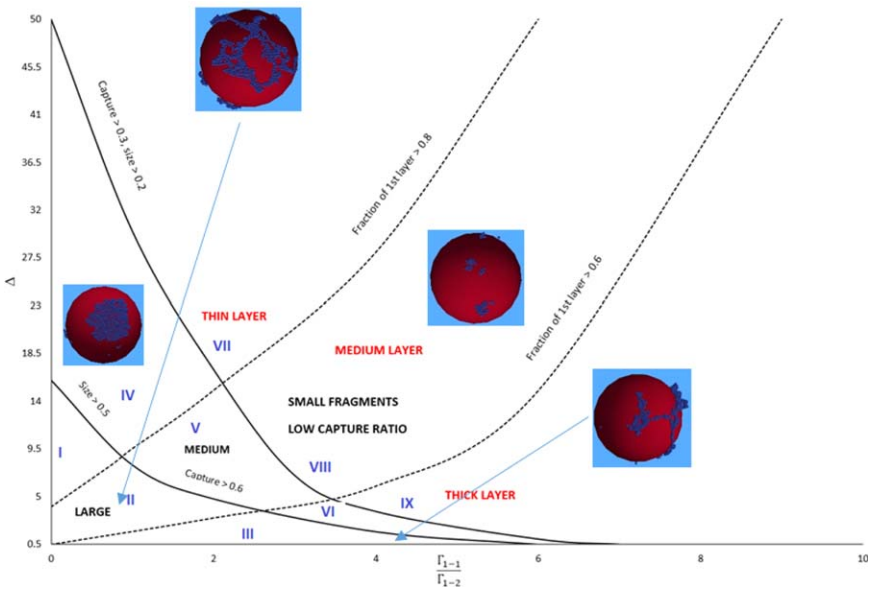

Figure 16. Breakage and adhesion regimes constructed by the dimensionless number Δ and interface energy ratio.

Nine regimes are distinguished based on the capture ratio, the fragment size, and the thickness of covering layer. [Color figure can be viewed in the online issue, which is available at wileyonlinelibrary.com.]

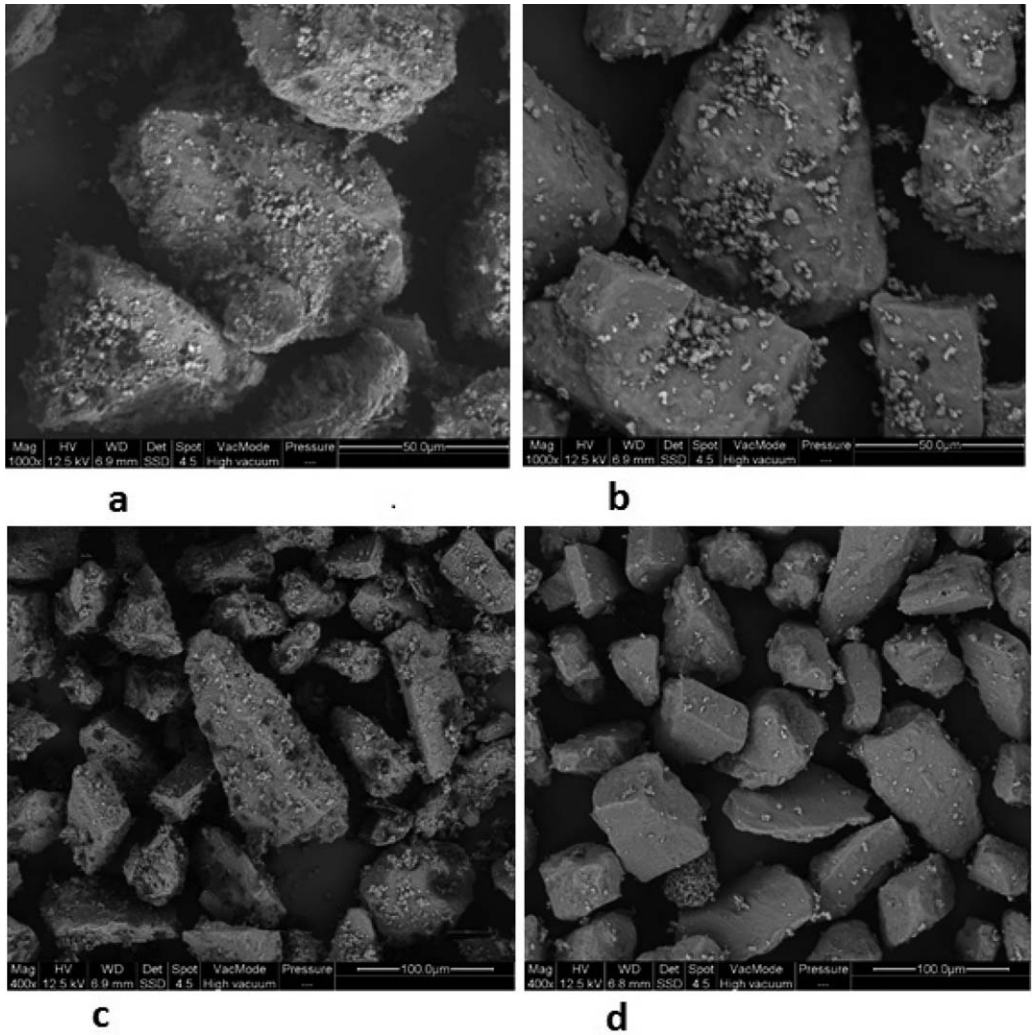

Figure 17. SEM images from adhesive mixtures of (a) uncoated lactose carrier, (b) Mgstearate coated carrier, (c) and (d) correspond to the case of short mixing time.

Effects of API-carrier interaction on the capture ratio and the API thickness can be observed.

surface was found in the case of higher mixing rate (1000 rpm). This observation can be translated to the variation of the Δ number, that is, along the *y*-axis in the regime map (Figure 16) where a thinner layer of fines is predicted at higher value of Δ (higher impact velocity). In addition, the size of fragments reflected by the regime map is also in agreement with the experiments, that is, lower mixing intensity results in larger fragments. The smearing effect of MgSt, as noted by the author, takes place at longer mixing times to form a thin film, consequently, the structure at early mixing time is solely affected by the adhesion of fines onto the carrier surface. This dependence of the covering layer on the mixing rate is also documented by Sato et al.[18]

According to the above experimental support, the simulation shows its feasibility in capturing and predicting key aspects of adhesive particle mixing using the dimensionless numbers.

With its potential in predicting the structure of breakage fragments, the constructed breakage–adhesion regime map can be used as a guide for selecting preliminary physical properties, for example, surface properties, and impact velocity (which can be related to the mixing speed) for different application purposes. For instance, the goal of dry particle coating is to obtain a continuous and even distribution of fines on the target,[18,19] consequently, a thin layer and a high capture ratio found in the regime I is preferable to utilize the fines load. Therefore, the formulation can be started at high $\Gamma_{1\text{-}2}$ (if possible) to keep the process operating at a low interface energy ratio. Although high impact velocity, that is, high mixing speed, leads to a thin layer, it should be adjusted in relation to $\Gamma_{1\text{-}1}$ to ensure sufficient adhesion of fines onto the target.

While the desired structure is evident in the case of a dry particle coating, the situation is more delicate for adhesive mixtures for inhalation. There is currently no efficient method for measuring the size or the strength of fine particle fragments that adhere to carrier particles. The fragments of API are, however, often observed in SEM images of adhesive mixtures, in particular at high drug loads and upon the addition of lactose fine particles to the formulations.[20,21] The use of specially made API agglomerates has been reported[22] and the formation of mixed agglomerates between API and lactose fines has been demonstrated using Time-Of-Flight Secondary Ion Mass Spectroscopy (TOF-SIMS) analysis.[23] Much research has been directed towards understanding the so-called "fines effect,"[2] which refers to the increase in fine particle fraction when lactose fine particles are added to adhesive mixtures for

inhalation. In depth studies performed by Kinnunen et al.[24] point to the coformation of fragments as the main reason for this effect. All of the above research indicates that fine particle fragments are beneficial to the delivery of inhaled drugs, the main reason being that a fine particle fragment is more easily released from the carrier by the inhalation air stream than individual particles attached to the carrier surface. To reach the lungs, the aerodynamic particle size should be less than about 5 μm. In many dry powder systems, the size of the API is about 2 μm, which means that small fragments can still be inhaled. Larger fragments should obviously be avoided, unless they are broken up by the turbulent airstream that occurs during inhalation. The mechanical strength of adhered fragments, however, is governed not only by surface properties but also by impact velocity. It was found, here, that the total force acting on fine particles is enhanced by the use of high impact velocity, for example, a high Δ number, which means that a larger amount of energy is needed to break the adhered fragments. According to the DEM-based analysis in this study, the mechanical strength of fragments is diminished at high $\Gamma_{1\text{-}1}$ due to restructuring mechanisms. Upon impact, the surviving fragments are compressed under the impact force, which results in greater strength than the original agglomerates. The use of high $\Gamma_{1\text{-}1}$, however, is a disadvantage in restructuring and causes an increase in packing density and tensile strength. Based on the above findings, the regimes that give a low capture ratio, that is, VII, VIII, and IX, are not a proper choice. The thin covering layer regimes, that is, I, IV, and VII, should also be avoided, as it blocks the removal of fines from the carrier surface. Most likely, the regime III is a suitable starting point, owing to its ability to facilitate the disintegration of large fines fragments.

Conclusions

This article presents the detailed analysis of the effects of interface energies on the impact of loose agglomerates with a spherical target using DEM simulations. The agglomerate breakage is found to be governed not only by the interaction between fine particles, that is, cohesion but also by the interaction between fine and carrier particles, that is, adhesion. Interestingly, the deposition of breakage fragments on the carrier surface is influenced by the relative importance between the two interface energies.

The coupling effect of the cohesion and the adhesion on the agglomerate impact motivates their integration in terms of a new dimensionless group, the ratio of the two interface energies which is suggested from a mechanistic approach. This new number, in combination with the dimensionless number Δ, makes it feasible to relate the impact behavior of the agglomerates to particle properties; and is used to construct a map in which different regimes are distinguished based on the desired structure of daughter fragments resulting from a breakage–adhesion event. With a good agreement with experimental observations, the regimes mapped in this work can be used as a guide for selecting preliminary operating conditions, not only in the context of agglomerate impacts but also in other processes having the same mechanisms owing to the utilization of the dimensionless numbers.

This work also reflects the need for further research, for example, exploring complex surface properties which is currently simplified, to give an overall picture of the agglomerates impact.

Notation

Roman letters

A = contact area between two particles, m^2
a = contact area between two particles, m^2
D = diameter of particle, m
e = restitution coefficient, Dimensionless
E = Young modulus, Pa
F_{ne} = elastic part of normal collision force, N
F_{ij} = interparticle contact force between particle i,j, N
k = proportionality factor, Dimensionless
m_i = mass of particle i, kg
N = number of particles in agglomerates, Dimensionless
N_B = number of broken interparticle bonds, Dimensionless
N_1 = number of bonds between fines and the target, Dimensionless
R = radius of particle, m
T_i = torque acting on particle i, Nm
V = impact velocity, ms^{-1}

Greek letters

Δ = dimensionless number relating kinetic energy to agglomerate strength[9], $\Delta = \frac{\rho D^{5/3} V^2 E^{2/3}}{\Gamma^{5/3}}$, Dimensionless
Γ = interface energy between two particles, J/m^2
v = Poisson ratio, Dimensionless
ω = angular velocity of particle, rad/s
ρ = particle density, kgm^{-3}

Acknowledgments

Simon Åslund is acknowledged for the preparation of API mixtures and Johan Arnehed for SEM pictures. Financial support from POWTECH ITN (Grant 264722) is gratefully acknowledged.

Literature Cited

1. Sauer D, Cerea M, DiNunzio J, McGinity J. Dry powder coating of pharmaceuticals: a review. *Intl J Pharma.* 2013;457(2):488–502.
2. Jones M, Price R. The influence of fine excipient particles on the performance of carrier-based dry powder inhalation formulations. *Pharm Res.* 2006;23(8):1665–1674.
3. de Boer AH, Chan HK, Price R. A critical view on lactose-based drug formulation and device studies for dry powder inhalation: which are relevant and what interactions to expect? *Adv Drug Delivery Rev* 2012;64(3):257–274.
4. Ghadiri M, Moreno-Atanasio R, Hassanpour A, Antony SJ. Analysis of agglomerate breakage. In: Agba D, Salman MG, Michael JH, editors. *Handbook of Powder Technology*, Vol 12, Chap 19. Amsterdam: Elsevier Science, 2007:837–872.
5. Sarkar A, Wassgren CR. Effect of particle size on flow and mixing in a bladed granular mixer. *AIChE J.* 2015;61(1):46–57.
6. Thornton C, Liu L. How do agglomerates break? *Powder Technol.* 2004;143–144:110–116.
7. Subero J, Ning Z, Ghadiri M, Thornton C. Effect of interface energy on the impact strength of agglomerates. *Powder Technol.* 1999; 105(1–3):66–73.
8. Moreno-Atanasio R. Energy dissipation in agglomerates during normal impact. *Powder Technol.* 2012;223:12–18.
9. Moreno-Atanasio R, Ghadiri M. Mechanistic analysis and computer simulation of impact breakage of agglomerates: effect of surface energy. *Chem Eng Sci.* 2006;61(8):2476–2481.
10. Thornton C, Yin K, Adams M. Numerical simulation of the impact fracture and fragmentation of agglomerates. *J Phys D: Appl Phys.* 1996;29(2):424.
11. Nguyen D, Rasmuson A, Thalberg K, Niklasson Björn I. Numerical modelling of breakage and adhesion of loose fine-particle agglomerates. *Chem Eng Sci.* 2014;116:91–98.
12. Johnson K, Kendall K, Roberts A. Surface energy and the contact of elastic solids. *Proc R Soc Lon A. Math Phys Sci.* 1971;324(1558): 301–313.
13. Thornton C, Ciomocos MT, Adams MJ. Numerical simulations of agglomerate impact breakage. *Powder Technol.* 1999;105(1–3):74–82.
14. Moreno R, Ghadiri M, Antony S. Effect of the impact angle on the breakage of agglomerates: a numerical study using DEM. *Powder Technol.* 2003;130(1):132–137.

15. Ester M, Kriegel H-P, Sander J, Xu X. A density-based algorithm for discovering clusters in large spatial databases with noise. Paper presented at Kdd. 1996;96(1):226–231.
16. Swaminathan V, Cobb J, Saracovan I. Measurement of the surface energy of lubricated pharmaceutical powders by inverse gas chromatography. *Intl J Pharm*. 2006;312(1–2):158–165.
17. Sato A, Serris E, Grosseau P, Thomas G, Chamayou A, Galet L, Baron M. Effect of operating conditions on dry particle coating in a high shear mixer. *Powder Technol*. 2012;229:97–103.
18. Sato A, Serris E, Grosseau P, Thomas G, Galet L, Chamayou A, Baron M. Experiment and simulation of dry particle coating. *Chem Eng Sci*. 2013;86:164–172.
19. Yang J, Sliva A, Banerjee A, Dave RN, Pfeffer R. Dry particle coating for improving the flowability of cohesive powders. *Powder Technol*. 2005;158(1–3):21–33.
20. Grasmeijer F, Hagedoorn P, Frijlink HW, de Boer AH. Drug content effects on the dispersion performance of adhesive mixtures for inhalation. *PLoS One*. 2013;8(8):e71339.
21. Grasmeijer F, Lexmond J, van den Noort M, Hagedoorn P, Hickey AJ, Frijlink HW, de Boer AH. New mechanisms to explain the effects of added lactose fines on the dispersion performance of adhesive mixtures for inhalation. *PLoS One*. 2014;9(1):e87825.
22. Ikegami K, Kawashima Y, Takeuchi H, Yamamoto H, Mimura K, Momose DI, Ouchi K. A new agglomerated KSR-592 β-form crystal system for dry powder inhalation formulation to improve inhalation performance in vitro and in vivo. *J Controll Release*. 2003;88(1):23–33.
23. Savolainen M, Nicholas M, Roos C, Josefson M, Fransson M, Petersson G, Thalberg K. Investigation of ordered mixtures using time-of-flight secondary ion mass spectrometry (TOF-SIMS). *RDD Europe*. 2013;2(1):243–246.
24. Kinnunen H, Hebbink G, Peters H, Shur J, Price R. Defining the critical material attributes of lactose monohydrate in carrier based dry powder inhaler formulations using artificial neural networks. *AAPS PharmSciTech*. 2014;15:1009–1020.

Manuscript received Mar. 6, 2015, and revision received May 8, 2015.